

Computer-Aided Detection of Breast Cancer Nuclei

Frank Schnorrenberg, *Student Member, IEEE*, Constantinos S. Pattichis, *Member, IEEE*,
Kyriacos C. Kyriacou, and Christos N. Schizas, *Senior Member, IEEE*

Abstract—A computer-aided detection system for tissue cell nuclei in histological sections is introduced and validated as part of the Biopsy Analysis Support System (BASS). Cell nuclei are selectively stained with monoclonal antibodies, such as the anti-estrogen receptor antibodies, which are widely applied as part of assessing patient prognosis in breast cancer. The detection system uses a receptive field filter to enhance negatively and positively stained cell nuclei and a squashing function to label each pixel value as belonging to the background or a nucleus. In this study, the detection system assessed all biopsies in an automated fashion. Detection and classification of individual nuclei as well as biopsy grading performance was shown to be promising as compared to that of two experts. Sensitivity and positive predictive value were measured to be 83% and 67.4%, respectively. One major advantage of BASS stems from the fact that the system simulates the assessment procedures routinely employed by human experts; thus it can be used as an additional independent expert. Moreover, the system allows the efficient accumulation of data from large numbers of nuclei in a short time span. Therefore, the potential for accurate quantitative assessments is increased and a platform for more standardized evaluations is provided.

I. INTRODUCTION

IN industrialized countries, breast cancer constitutes the most frequent malignancy among the female [1] population. It is estimated that one woman in eight will eventually develop the disease and about one third will die because of it. Despite being afflicted with this serious disease, patients with breast cancer exhibit a wide variation in prognosis and survival. One of the most important and favorable prognostic factors is the presence of steroid receptors for estrogen and progesterone in tumor cell nuclei. The objective of this study is to introduce and validate a computer-aided system for the detection of breast cancer nuclei, which is part of the Biopsy Analysis Support System (BASS) [1]. BASS was designed to facilitate the computer-aided classification and assessment of breast cancer immunocytochemical slides.

Demonstration of steroid receptors is routinely carried out by immunocytochemical methods which are performed on histological slides of biopsy specimens [2]. These slides are then assessed by an expert, in this case a histopathologist, who assigns a diagnostic index based on the intensity of stain

and the percentage of positive nuclei. The diagnostic index carries clinically important and highly significant information, since it is used by oncologists to formulate modes of treatment of individual cancer patients in an attempt to prolong patient survival. Consequently, there is a need to increase the accuracy of the diagnostic index beyond the limit of the human expert who at best can only assess microscopical images on a semi-quantitative subjective scale.

There are several sources of variation inherent in the immunocytochemical detection of breast cancer nuclei. These include variations in section thickness within and in between sections, inconsistencies due to different persons performing the techniques, variations in lighting across the optical field, as well as inter- and intraobserver variations [3]. To minimize some of the above variations and in an attempt to make the manual assessment of immunocytochemical slides more objective, a number of diagnostic schemes, such as the diagnostic index [4] and the closely related H-Score [5], have been introduced. Basically, the diagnostic index gives an evaluation of two variables as mentioned above, namely the staining intensity of tumor nuclei and the percentage of nuclei that are stained at a particular intensity (see also Appendix A). This strategy enables a semi-quantitative score to be calculated and is the method of choice being widely applied for the manual assessment of prognostic information related to immunocytochemistry.

Although, inter- and intra-observer variations are inherent in the manual evaluation methods, previous studies demonstrated the clinical importance of the semi-quantitative diagnostic index. Bosman *et al.* [6] also reported the usefulness of the semi-quantitative diagnostic index for interlaboratory comparisons and Jagoe *et al.* [7] reported that for immunolabeled tissue the intraobserver variation was twice as big as interobserver variation. Therefore, they concluded that in order to increase discrimination, it is preferable to have more observers assess a field than to ask one observer to assess one field multiple times.

In recent years, various computer-aided image analysis systems, such as CAS [8] and SAMBA [9], have been commercially developed for the purpose of quantifying the information from immunocytochemistry. These systems, however, although dedicated, do not use the manual approach of counting individual nuclei, but rather work with specific areas of stained nuclei [10]–[13]. This is because the identification of individual nuclei makes the accumulation of a reasonable sample size tedious and time consuming, since it is difficult to decide automatically or by visual inspection, whether nuclei touch or are partially overlapping [14]. To overcome these difficulties methods based on assessment of areas of interest (e.g. specifically stained nuclei) have been developed, which do not

Manuscript received December 2, 1996; revised May 18, 1997. This work was supported by a grant from the University of Cyprus. Additional support was provided by the Cyprus Planning Bureau, the General Secretariat of Research and Technology of Greece, and The Cyprus Institute for Neurology and Genetics.

F. Schnorrenberg, C. S. Pattichis, and C. N. Schizas are with the Department of Computer Science, University of Cyprus, CY-1678 Nicosia, Cyprus (e-mail: csfranks@turing.cs.ucy.ac.cy; pattichi@turing.cs.ucy.ac.cy; schizas@turing.cs.ucy.ac.cy).

K. C. Kyriacou is with the Department of Electron Microscopy, The Cyprus Institute of Neurology and Genetics, Nicosia, Cyprus.

Publisher Item Identifier S 1089-7771(97)06348-6.

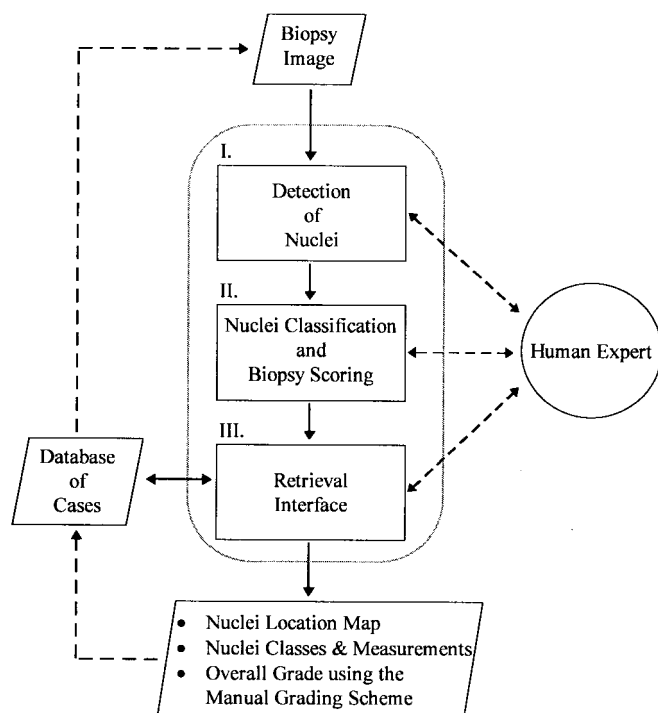


Fig. 1. Diagram of the Biopsy Analysis Support System (BASS).

rely on identifying individual nuclei. Additionally, methods depending on global thresholds to distinguish between stained tissue (specific staining) and background (nonspecific staining), are based on the assumption that local variations due to preparation or imaging do not significantly influence the measurements [10]–[14].

Furthermore, one of the main objectives of computer-aided biopsy analysis is to minimize some of the variabilities that occur as a consequence of the manual microscopical inspection of stained slides. In addition, computer-aided nuclei analysis also has to be efficient, since pathologists are unlikely to spend more time on evaluating a specimen than that required for the routine manual assessments. As already mentioned, in the manual assessment of biopsy slides one strategy has been to utilize a semi-quantitative scheme to make the assessment more accurate and more objective. To the best of our knowledge no systems as yet exist which attempt to aid the expert in the detection, counting, and classification of individual nuclei using the semi-quantitative scheme. The BASS system was designed to fill this gap, since commercially available computer-aided systems, such as CAS and SAMBA, are based on global thresholding techniques for discriminating between positive and negative nuclei.

The complete BASS system is illustrated in Fig. 1. It consists of the following three modules: 1) detection of nuclei; 2) nuclei classification and biopsy scoring; and 3) retrieval interface. The objective of this study is to introduce and validate BASS detection algorithm (top of Fig. 1). It enables the detection of individual immunocytochemically labeled nuclei in histological sections from breast cancer tumors by adapting to local and global image conditions. Breast cancer nuclei can be quite distinct and circumscribed in sections, but

vary in their average staining intensity. This makes them good candidates for detection by a matching operator using general geometrical constraints if the staining intensity variations can be sufficiently discounted. Moreover, methods using localized operators to detect and count nuclei consider only a small image area at a time. Thus, it is possible to adapt to locally varying conditions and consider global image statistics. In addition, the expert may apply his overall knowledge and experience regarding tissue structure to guide the system in the context of detecting scores of nuclei or even individual nuclei. BASS classifies the detected nuclei and computes the diagnostic index (middle of Fig. 1) as given in [1]. Finally, the assessment results are stored via the retrieval interface (Fig. 1, bottom) in the database of cases.

The material used in this study is described in Section II. Section III contains the description of the nuclei detection algorithm, while in section IV the results of the validation experiments are presented. Section V, finally, discusses the results.

II. MATERIAL

Eighteen breast cancer biopsy cases, immunolabeled for estrogen or progesterone receptors (ERICA-kit, Abbott, U.K.) and counterstained with haematoxylin to contrast positively stained nuclei (brown color) with negative nuclei (blue color), were chosen as the basis for this experiment. A medical expert selected and digitized up to three regions of interest from each slide at $\times 400$ magnification (Zeiss Axiophot microscope, SONY DXC-980P camera) in 24-bit color and 640×480 -pixel spatial resolution to appropriately sample each specimen. Each image was captured under the same reproducible conditions as follows: 1a) the microscope's field of view illumination was adjusted before every capture session with respect to the image frame size to give homogeneous lighting across the captured field of view, 1b) the light intensity and color temperature were fixed at the same values, 1c) the microscope was switched on at least 10 min before capturing started to allow the equipment to reach thermal equilibrium, 2a) the white and black balance of the camera were adjusted using a blank slide and blocked light passage to ensure an optimal use of the dynamic range of the camera, 2b) all other camera parameters were fixed, and the gamma correction of the camera was switched off (linear RGB), and 3) the room containing the capture equipment was darkened to minimize interference of ambient light with the capture process. Furthermore, at the beginning of each capture session one so called light distribution (ldist) image was captured using a complete slide except for the missing tissue specimen. Ldist images may be used to perform further corrections on the captured biopsy images with respect to intensity and chromatic aberrations of the capture system. In total, 28 images were captured and analyzed. All biopsy slides considered here were independently assessed for staining intensity and heterogeneity of nuclei using the routine laboratory procedure [4]. As a result of the routine manual assessment an overall grade, called diagnostic index, was assigned to each biopsy slide as given in Appendix A.

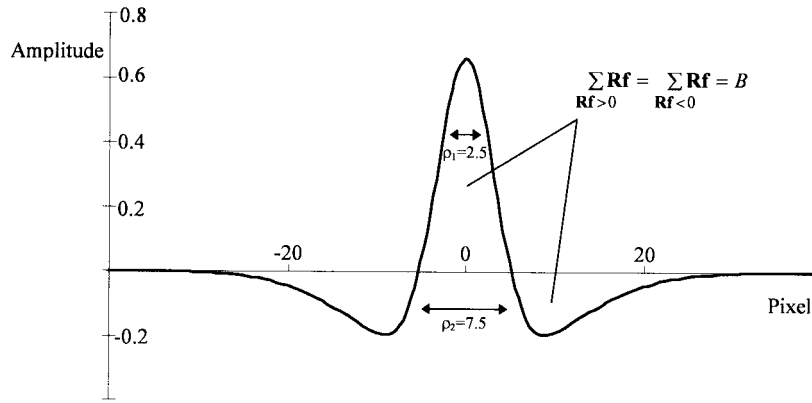


Fig. 2. One-dimensional (1-D) realization of the two-dimensional (2-D) receptive field described in (1).

III. NUCLEI DETECTION SYSTEM

In this section the mathematical background and the algorithmic description of the nuclei detection system are reported. Then, the classification algorithm is briefly outlined and the methods used to validate the nuclei detection system are presented.

A. Background

BASS' nuclei detection algorithm (top of Fig. 1) is based on the iterative application of a receptive field and a nonlinearity working as a localized operator and a soft threshold on the image, respectively. The algorithm transforms the optical density distribution of the original color image into a bimodal distribution where one mode is attributed to the background and the other mode is attributed to candidate nuclei. The minimum between the two modes is used to threshold the image allowing the detection of candidate nuclei. Thereafter, the centers of the candidate nuclei are located and reported.

Receptive fields based on differences and derivatives of gaussians are well known from biological vision [15]–[17] as well as image processing [18], [19]. A particular advantage of receptive fields based on gaussians is the fact that the filters are localized both in the spatial and frequency domains. Moreover, they can also be conveniently scaled to accommodate optimal response in a desired range of spatial scales. Thus, receptive fields can be well utilized as part of the nuclei detection system. In this study, the receptive field filter was designed to match nuclear shape and minimal proximity to neighboring image structure, i.e., isolated nuclei versus touching nuclei. In a convolution operation with the image, objects closely matching the receptive field were enhanced, while the rest of the image structure was suppressed. The receptive field was implemented as follows (see also Fig. 2):

$$Rf(x, y) = B \cdot \left\{ \alpha \cdot \exp\left(-\frac{x^2 + y^2}{2\rho_1^2}\right) - J \cdot \exp\left(-\frac{x^2 + y^2}{2\rho_2^2}\right) \right\} \quad (1)$$

where B , α , ρ_1 , ρ_2 , and J are constants. The parameters ρ_1 and ρ_2 determine the sensitivity of the filter regarding the range of object sizes. B is an amplification constant which ensures that

the receptive field response to matching image structure with low intensity values (s_{\min}) is higher than the offset value of the squashing function (see (5) below). The offset value can be thought of as a watershed dividing potential background from candidate nuclei. B is chosen as

$$B = \text{offset}/s_{\min}. \quad (2)$$

The constant α ensures that the positive (excitatory) values of the receptive field add to unity, assuming B is 1:

$$\alpha = (\sum [Rf(x, y) > 0])^{-1}. \quad (3)$$

J is computed so that excitatory and inhibitory components of the receptive field cancel (zero DC):

$$J = \frac{\sum \alpha \cdot \exp\left(-\frac{x^2 + y^2}{2\rho_1^2}\right)}{\sum \exp\left(-\frac{x^2 + y^2}{2\rho_2^2}\right)}. \quad (4)$$

A nonlinear squashing function is applied to the result of the convolution of the receptive field and the image to make a soft decision concerning how each pixel should be labeled 1) background, i.e. minimal intensity, or 2) object, i.e. maximal intensity. It is a soft decision, because the squashing function will not assign one out of two values to all pixels, as would be the case when using a step function. Instead, the squashing function transforms the intensity distribution of the convolved image into a bimodal distribution. Repeated application of the receptive field/squashing function combination transforms the image in the limit into a binary array, labeling each pixel value as belonging to the background or an object. The system uses a squashing function as follows (see also Fig. 3):

$$Sq(I_k) = \frac{\text{scale}}{1 + \exp[-\text{incl} \cdot (I_k - \text{offset})]} \quad (5)$$

where scale determines the range of the function, incl determines the inclination, and offset determines the offset along the abscissa. These parameters are defined as follows:

$$\text{scale} = s_{\max} - s_{\min}, \quad (6)$$

$$s_{\max} = \max(I_k) - d_k \quad (7)$$

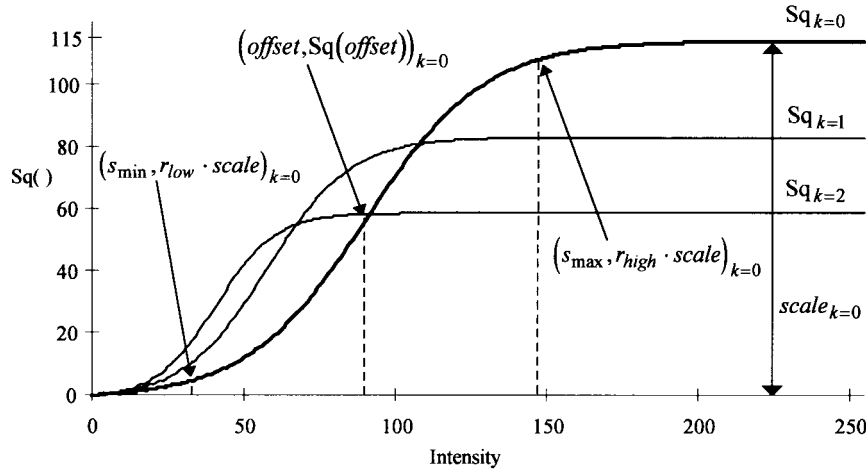


Fig. 3. Squashing function (5) realization for three iterations: For $k = 0, 1, 2$, $s_{\min} = 32.54, 16.92, 11.95$, $s_{\max} = 147.67, 92.22, 69.35$, $r_{\text{low}} = 0.05, 0.05, 0.05$, $r_{\text{high}} = 0.95, 0.95, 0.95$, $\text{scale} = 115.14, 81.30, 57.41$, $\text{offset} = 90.11, 57.57, 40.65$, and $\text{incl} = 0.051, 0.072, 0.103$, respectively.

where k is the index of the current iteration $k > 0$,

$$s_{\min} = \min(I_k) + d_k, \quad (8)$$

$$d_k = \begin{cases} \text{S.D.}(I_k), & \text{for } k = 0, \\ d_{k-1} \cdot \frac{\max(I_k) - \min(I_k)}{\max(I_{k-1}) - \min(I_{k-1})}, & \text{for } k < 0 \end{cases} \quad (9)$$

$$\text{offset} = s_{\min} + \frac{\text{scale}}{2}, \quad (10)$$

$$\text{incl} = 2 \frac{\ln(r)}{\text{scale}}, \quad (11)$$

$$r = \frac{r_{\text{high}}}{r_{\text{low}}} = \frac{0.95}{0.05}. \quad (12)$$

It can be shown that the linear portion of the squashing function slope, that is the first derivative of the squashing function evaluated at offset, takes on a value of

$$Sq'(\text{offset}) = \frac{\ln(r)}{2} \approx 1.47 \quad (13)$$

due to the parametrization of the squashing function. Thus the slope of the squashing function at offset is about 74° .

The algorithmic constant d_k is given by the image standard deviation (SD) in the first iteration, whereas in the following iterations it is computed as a fraction of d_{k-1} . The constant d_k is used to adjust the s_{\min} and s_{\max} parameters, which in turn are essential in the parametrization of the squashing function. The key to the chosen parametrization of the squashing function are the desired squashing function values for s_{\min} and s_{\max} . The interval between s_{\min} and s_{\max} defines the decision region where the magnitude of the receptive field response determines whether pixel intensities are squashed towards the minimum or the maximum. $Sq(s_{\min})$ and $Sq(s_{\max})$ are proportional to the constants r_{low} and r_{high} and the scale parameter

$$\begin{aligned} Sq(s_{\min}) &= r_{\text{low}} \cdot \text{scale} \\ Sq(s_{\max}) &= r_{\text{high}} \cdot \text{scale}. \end{aligned} \quad (14)$$

Repeated application of the receptive field and the squashing function to the image ensures that object detection is mostly dependent on object geometry and not on object intensity

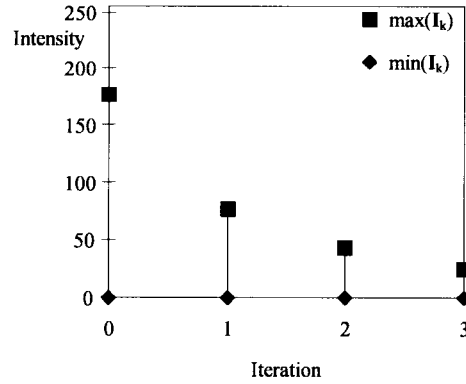


Fig. 4. Development of the intensity range of a biopsy image over three iterations: iteration 0 signifies the original intensity range, while iterations 1 to 3 specify the range after the iterations.

(see also Appendix B for an analysis of the receptive field response related to object size). The iterations can be stopped and a threshold can be determined when the image histogram has become distinctly bimodal. Fig. 4 and Fig. 5 present the development of the intensity range and the intensity distribution of a sample biopsy image over three iterations, respectively. The intensity range clearly shrinks, while at the same time a bimodal distribution develops.

The histogram vector is smoothed with a moving average filter which is chosen to be insensitive to local minima. The threshold value T is set equal to the histogram bin with the minimum amount of pixels between the two modes of the histogram:

$$T = \min_{\text{mode}}(\text{hist}(I) \otimes [a_0, \dots, a_{0.3 \cdot \text{scale}-1}]) \quad (15)$$

where $\text{hist}(I)$ returns the histogram of I , $a_0, \dots, a_{0.3 \cdot \text{scale}-1} = |0.3 \cdot \text{scale}^{-1}|$ define the moving average filter coefficients, \min_{mode} returns the minimum between two maxima, which is used to obtain the corresponding threshold intensity, T . The threshold value T is used to segment the sample image into background and candidate nuclei. The candidate nuclei in the image, i.e. all connected sets of pixels, are recorded in an object

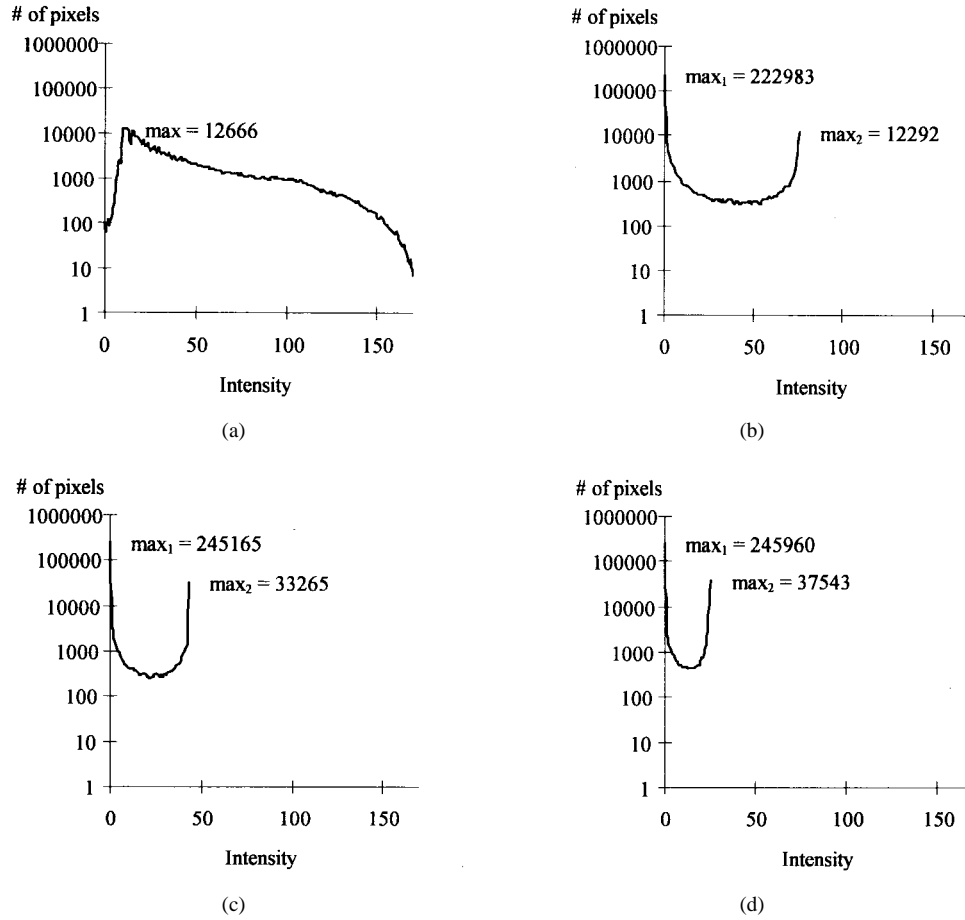


Fig. 5. Development of the histogram vectors of a biopsy image over three iterations: (a) original histogram of the biopsy image (iteration 0), (b) iteration 1, (c) iteration 2, and (d) iteration 3.

list. Depending on user preference, the object list can automatically be revised with respect to a specified roundness threshold. Roundness is defined as

$$\text{roundness} = \frac{\text{perimeter}^2}{4\pi \cdot \text{area}} \quad (16)$$

where perimeter are perimeter pixels, determined by morphological operations [20], and area is the area of one candidate nucleus. Finally, the nuclei center locations are computed and returned.

B. Detection Algorithm

BASS' nuclei detection algorithm is mainly data driven. It can be applied to a series of images without user interaction, because the algorithm adapts to local and global imaging conditions automatically. In this subsection, the detection algorithm is presented.

Step 1) Correct Color Image for Inhomogeneous Lighting: The color image as well as the associated *ldist* image (see section II) are transformed from RGB colorspace to the more intuitive Hue-Lightness-Saturation (HLS) color space [21] to facilitate the correction process. The *ldist* image is considered the reference white standard image. Under this assumption spatial intensity and color variations due to the imaging system may be corrected by normalizing each pixel in the color image

with respect to the *ldist* image. In particular, saturation, and lightness may be corrected using the fact that they should be zero and one in the *ldist* image. Moreover, observed standard deviations in the region of 3% and 9% for pixel values in the lightness and saturation channels of a typical *ldist* image let a normalizing correction of the respective values in the color image appear even more desirable. The color image's additive saturation (*S*) and lightness (*L*) coordinates are corrected as follows, while polar hue coordinate is not considered here:

$$S'(x, y) = S(x, y) / (S_{ldist}(x, y) + 1) \quad (17)$$

$$L'(x, y) = L(x, y) / L_{ldist}(x, y) \quad (18)$$

where $0 \leq S, L \leq 1$. Subsequently, the color image is transformed back into RGB color space. It should be noted that the color image transformation described here was mainly conceived to aid further processing, but also leads to visually pleasing results.

Step 2) Convert Color Image to Optical Density Image: The original RGB color image is transformed into a scalar array, *I*, using the inverted Y channel (optical density) of the RGB-YUV transform [22] to accommodate the on-center-off-surround type receptive field detection characteristics:

$$I(x, y) = 255 - [0.222 \quad 0.707 \quad 0.071] \cdot \begin{bmatrix} R(x, y) \\ G(x, y) \\ B(x, y) \end{bmatrix} \quad (19)$$

where $0 \leq I, R, G, B \leq 255$. The Y channel approximately captures the sensitivities of the human visual system with respect to perceived optical density of each color (luminous efficiency).

Step 3) Compute the Receptive Field Array: The receptive field array given in (1) is calculated according to the specified parameters ρ_1, ρ_2 , and the derived parameters B, α , and J , given in (2), (3), and (4) respectively. The parameters ρ_1 and ρ_2 were fixed at 2.5 and 7.5, respectively. In general, small variations in the parameters ρ_1 and ρ_2 will lead to minimal performance changes.

Step 4) Apply Iteratively the Receptive Field and the Squashing Function:

```

WHILE ( $k < 3$ ) DO
  ADJUST  $d_k$ , scale, offset, incl
   $I'_k = Rf \otimes I_k$ 
  IF  $\max(I'_k) > \min(I'_k)$  THEN
     $I_{k+1} = Sq_k(I'_k)$ 
  ELSE
    PRINT "No nuclei found"
    EXIT
  ENDIF
ENDWHILE

```

(20)

where I_k and Sq_k depict the image array and the squashing function given by (5) at the k th iteration. At the beginning of each iteration the squashing function parameters scale, offset, and incl are adjusted according to the current image array and the previous parameter values. Then, the image is convolved with the receptive field. If the maximum of the image is greater than the minimum, the image is squashed, otherwise no nuclei were found. Within three iterations the image intensity distribution takes on a bimodal shape, clearly indicating the presence of two pixel classes: (i) background, and (ii) candidate nuclei.

Step 5) Threshold Bimodal Histogram: The bimodal image histogram is smoothed and the intensity value corresponding to the minimum between the two modes is computed. Histogram smoothing is performed with a moving average filter and thereafter, the image is thresholded using the calculated intensity value given in (15). The candidate nuclei are now represented in an image array as disconnected sets of pixels with maximal intensity. These sets are explicitly registered in a list of candidate nuclei.

Step 6) Revise and Return the List of Detected Nuclei: Depending on user preference, the candidate nuclei list can now automatically be revised with respect to a specified roundness threshold [20]. The roundness threshold was set equal to zero for this study to avoid discarding any objects based on the shape. Finally, for each nuclei the center location is computed and returned.

C. Classification Algorithm [1]

Following the detection of nuclei, the classification algorithm is applied to classify each nucleus into one of five staining intensity classes. After the classification of each nucleus, the diagnostic index is computed as illustrated in

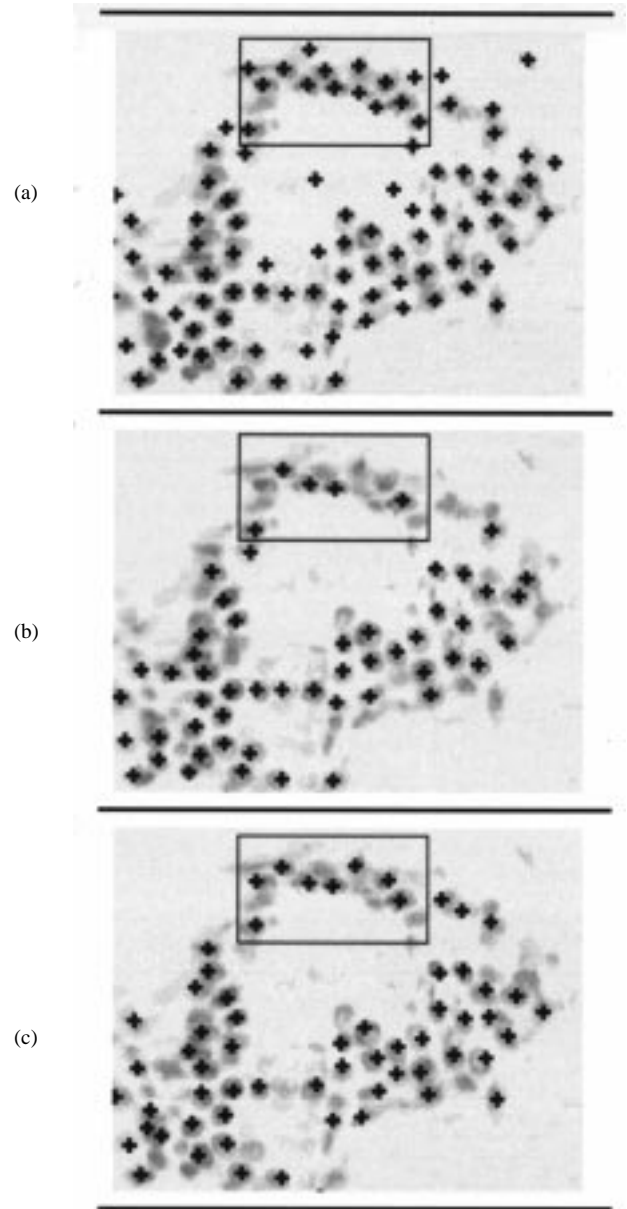


Fig. 6. Example of nuclei detection: (a) BASS' detection system, (b) Expert 1, and (c) Expert 2. Detected nuclei are marked with crosses, and it is shown that in the region outlined by the black frame BASS detected more nuclei.

Fig. 8. The classifier was trained and tested on the mask images (see Section III-D) created by one of the experts. A more detailed description of the classification stage can be found in [1]. The main steps of the classification algorithm are summarized as follows:

Step 1) Extract Features for Each Nucleus: The following local and global features are extracted: i) Local features: the average of the Y, U , and V channel as well as a texture measure are computed for each nucleus and ii) Global features: the average and variance of the Y channel are computed for all nuclei in the image.

Step 2) Classify Each Nucleus: A nucleus is classified into one of five staining intensity classes (negative, weak, moderate, strong, very strong) using the radial basis function neural network classifier. The RBF nets [23] were trained using an

incremental solver [24], which dynamically adds RBF neurons to the network and adjusts the weights until either a maximal number of neurons has been added or the sum-squared error falls beneath an error goal. The transfer function (TF) of each RBF neuron has the following form:

$$TF(\mathbf{p}) = \text{RBF}(\text{dist}(\mathbf{w}, \mathbf{p}) * 0.8326/SP) \quad (21)$$

where \mathbf{p} is the input feature vector, \mathbf{w} is the weight vector, dist is the Euclidean distance measure, SP is the spread constant, and RBF is a Gaussian function. The transfer function TF (21) takes on its maximal value to 1 when its argument becomes zero. The RBF function will return 0.5 when its argument has the value 0.8326. Thus, TF will be one, if the distance between the vectors \mathbf{p} and \mathbf{w} is zero. If, for example, the spread constant SP equals to 0.1, TF would return 0.5 for every vector at a distance of 8.326 from \mathbf{w} . The best architecture achieved 72% correct classifications and consisted of 100 neurons using a spread constant of 20.

Step 3) Compute Diagnostic Index: The diagnostic index is computed according to the manual semi-quantitative scheme which is described in Appendix A.

D. System Validation

To create a basis for comparison, a small circular probe (9.5 pixels) was placed centrally on top of each nucleus detected by BASS' detection algorithm. Independently, two experts placed the same sized probes manually where they perceived the nuclei centers were located using the mouse interface. In addition, the probes were color coded depending on the staining intensity class computed by BASS' classification algorithm described in Section III-C or assigned by the expert. As a result of this procedure, three mask images were created, one for the system and one for each expert. The diagnostic index for both the system and the experts was automatically computed according to , using the above described color coded mask images.

A detection event was defined as the set of pixels belonging to one of the probes in the image. If two probes from different mask images overlapped, the two corresponding detection events were said to coincide and the corresponding nucleus was interpreted to have been detected in both mask images. In the case of one probe touching several other probes, only one coinciding detection event was counted. A hybrid, called the *OR-ed expert*, was derived with a modified logical OR operation from the individual experts' masks. The modification of the OR concerned overlapping nuclei probes, in which case a new probe was placed on top of the center of overlapping probes and the rest of the probes were erased.

System validation was performed using three methods. In particular, the detection algorithm performance and the joint detection and classification performance of the BASS system were assessed with the following methods:

- 1) Receiver-operator characteristic measures (ROC) were used to analyze individual nuclei detection performance of the BASS system compared to that of two experts. ROC measures are useful to compare the detection performance with respect to individual nuclei because no

assumption about the underlying probability distribution of the detection events is made. Based on the definition of the detection events, two measures, sensitivity (SS) and positive predictive value (PPV), were chosen to characterize the detection performance.

Sensitivity is the likelihood that a nucleus will be detected in case it is also marked as a nucleus in the gold standard. It is defined as follows:

$$SS = TP/(TP + FN) \quad (22)$$

where TP (true positive) are those nuclei marked in both the gold standard and the image, and FN (false negative) are those nuclei which are marked in the gold standard, but not in the image.

Positive predictive value (PPV) is the likelihood that the detection of a nucleus is actually associated with a nucleus marked in the gold standard.

$$PPV = TP/(TP + FP) \quad (23)$$

where FP (false positive) are those nuclei which are marked in the image, but not in the gold standard.

- 2) Spearman's rank-order correlation coefficient was determined to assess the joint performance of BASS' detection and classification system compared to that of two experts based on the staining intensity class proportions of all biopsy images [25]. The coefficient makes no assumptions about the underlying probability distributions and since proportions are analyzed, the measurements are independent of the absolute numbers of detected nuclei. On average about 180 nuclei were detected in each image by the system, while the experts marked on average about 115. However, bias toward one or the other nuclei class or staining intensity, is registered by the Spearman's rank-order correlation coefficient. This is a relative bias due to the lack of gold standards. The Spearman's rank-order correlation coefficient is given by [26]

$$r_s = \frac{\sum_{i=0}^{N-1} (Rx_i - \overline{Rx})(Ry_i - \overline{Ry})}{\sqrt{\sum_{i=0}^{N-1} (Rx_i - \overline{Rx})^2} \sqrt{\sum_{i=0}^{N-1} (Ry_i - \overline{Ry})^2}} \quad (24)$$

where \mathbf{X} and \mathbf{Y} are vectors containing the proportions of a particular staining intensity class for all biopsy images, and Rx_i and Ry_i are magnitude based ranks among \mathbf{X} and \mathbf{Y} , respectively.

- 3) Confusion matrices were used to evaluate the experts' and BASS' performance in the assessment of diagnostic indices as compared to the routine diagnostic index. The confusion matrices show where and how much two classification results deviate from each other. The

TABLE I
COMPARISON OF BASS AND TWO EXPERTS WITH RESPECT TO
SENSITIVITY (SS) AND POSITIVE PREDICTIVE VALUE (PPV),
WHERE THE GOLD STANDARD IS INDICATED WITH AN “*”

	SS \pm S.D. %	PPV \pm S.D. %
Expert 1 – Expert 2*	72.6 \pm 15.1	74.5 \pm 14.3
BASS – Expert 1*	84.6 \pm 14.7	54.5 \pm 15.6
BASS – Expert 2*	83.7 \pm 14.0	55.8 \pm 18.6
BASS – <i>OR</i> -ed Expert*	83.0 \pm 14.5	67.4 \pm 14.2

confusion matrices are defined as follows:

$$\mathbf{M}_C = \begin{bmatrix} c_{0,0} & & c_{0,4+} \\ & \cdot & \\ & & \cdot \\ c_{4+,0} & & c_{4+,4+} \end{bmatrix} \quad (25)$$

where $c_{j,k}$ = “Percentage of cases relative to the whole database with diagnostic index k (column index) classified as j (row index)”, $j, k = 0, \dots, 4+$.

IV. RESULTS

A. Detection Example

Fig. 6 shows a subregion of a breast cancer biopsy image. In Fig. 6(a) nuclei detected by BASS are marked, whereas Fig. 6(b) and (c) present the detection results from expert 1 and expert 2, respectively. The black frame inserted in each figure, indicates a region of the image comparing assessments by BASS, expert 1, and expert 2. BASS generally detected more nuclei in the biopsy images than both experts.

B. ROC Analysis

Table I shows the ROC measures SS and PPV obtained from four experiments based on a total of 28 images from 18 breast cancer cases: this compares the performance of BASS to expert 1, expert 2, and the *OR*-ed expert. The experts were also compared to each other. It should be noted that to reverse the roles of the gold standard and specimen image, it is sufficient to reverse the labels for SS and PPV. When the two experts were compared to each other, the experts’ SS and PPV values were 72.6% and 74.5%, respectively. The PPV values indicate that at least 25% of the nuclei were mutually not detected by the experts. BASS, when compared to each expert, achieved a higher sensitivity score of at least 83.7%, but a lower PPV in the region of 55%. This indicates that about 45% of the nuclei detected by the system were in fact not identified as such by the individual experts. When comparing BASS with the *OR*-ed expert, the sensitivity score increased only slightly. However, the PPV value increased by about 12% to 67.4%. This clearly illustrates that BASS’ performance is more consistent with

the *OR*-ed expert performance. The better PPV value was due to considerably less false positive detection by BASS, because the *OR*-ed expert detection results contained generally more detected nuclei. Fig. 7 presents corresponding scatter plots regarding these measures of all cases in the biopsy slide database. It is clearly shown that due to the subjective nature of the manual assessment there is a wider scatter when comparing the results obtained by the two experts [Fig. 7(a)] than the results obtained by BASS versus each expert [Fig. 7(b) and (c)]. In this respect, the least scatter was obtained when BASS was compared to the *OR*-ed expert [Fig. 7(d)].

C. Spearman’s Rank Order Correlation Analysis

Table II shows the results of Spearman’s rank order correlation analysis of the proportion of each staining intensity class (negative, weak, moderate, strong, very strong) in all images as classified by BASS versus the experts. The two-sided significance based on a 5% level is indicated with an asterisk next to the coefficient. The experts’ overall assessments were moderately correlated (>0.65) except for weakly stained nuclei, where the value of correlation coefficient was only 0.32. The nuclei staining intensity proportions assigned by BASS correlated strongly (>0.78) with each expert for strongly and very strongly stained nuclei; while for the weakly stained nuclei the correlation was lowest with 0.51 and 0.38, respectively.

D. Confusion Matrix Comparison of Biopsy Grading Performance

Table III shows three confusion matrices comparing the routine diagnostic indices with: (a) BASS, (b) expert 1, and (c) expert 2. The entries of the matrices are given as percentage values, where 100% is equivalent to all breast cancer cases in the biopsy database. The last row at the bottom of each matrix illustrates the percentage of the breast cancer cases in each diagnostic index category. For example, with reference to Table III(a) 25.0% of the cases in the database were assigned a routine diagnostic index of 2+, while BASS classified 10.7% of the cases as 2+ and 14.3% of the cases as 3+. BASS displayed a weakness by either overscoring or underscoring 3+ routine diagnostic index cases. It is apparent that BASS performed best for biopsy slides with routine diagnostic indices of 1+ and 4+ respectively. In general, the experts showed a tendency to overscore, but for the 1+ routine diagnostic index category both experts underscored or overscored all cases as shown in Table III(b) and (c). Both the experts and BASS overscored all 0 routine diagnostic index cases.

V. DISCUSSION

An algorithm for detecting immunocytochemically labeled nuclei in histological sections from breast cancer tumors was introduced and validated in this study as part of the BASS. BASS is a system which aims to provide computer-aided support for enabling a more efficient and accurate detection of breast cancer nuclei based on their staining intensity and number of nuclei stained. This task is generally deemed to be quite difficult, since tissue sections constitute a very complex medium that hampers efforts to streamline and standardize

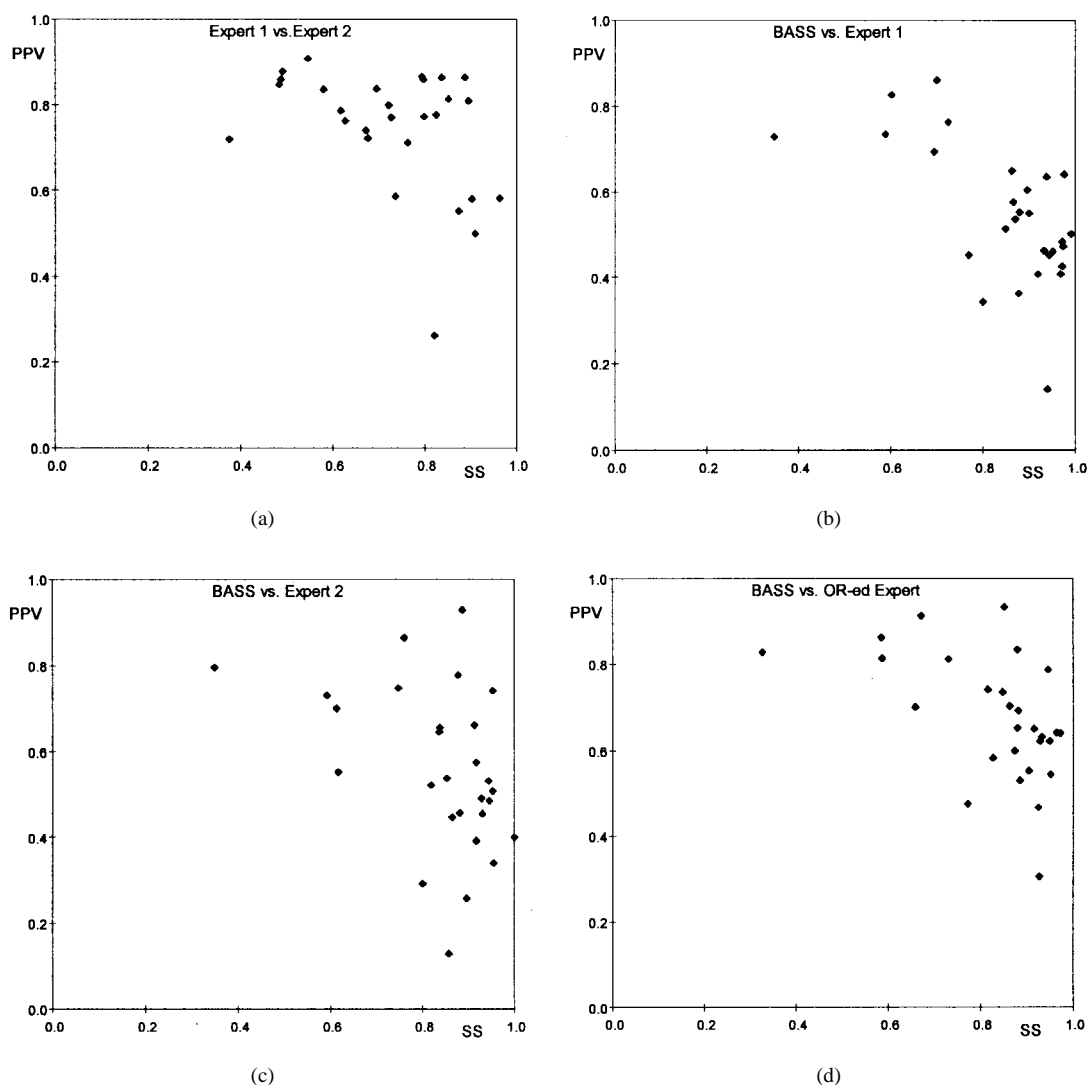


Fig. 7. Scatter plots of positive predictive value (PPV) versus sensitivity (SS) illustrating the performance of (a) BASS, (b) Expert 1, (c) Expert 2, and (d) the *OR*-ed expert.

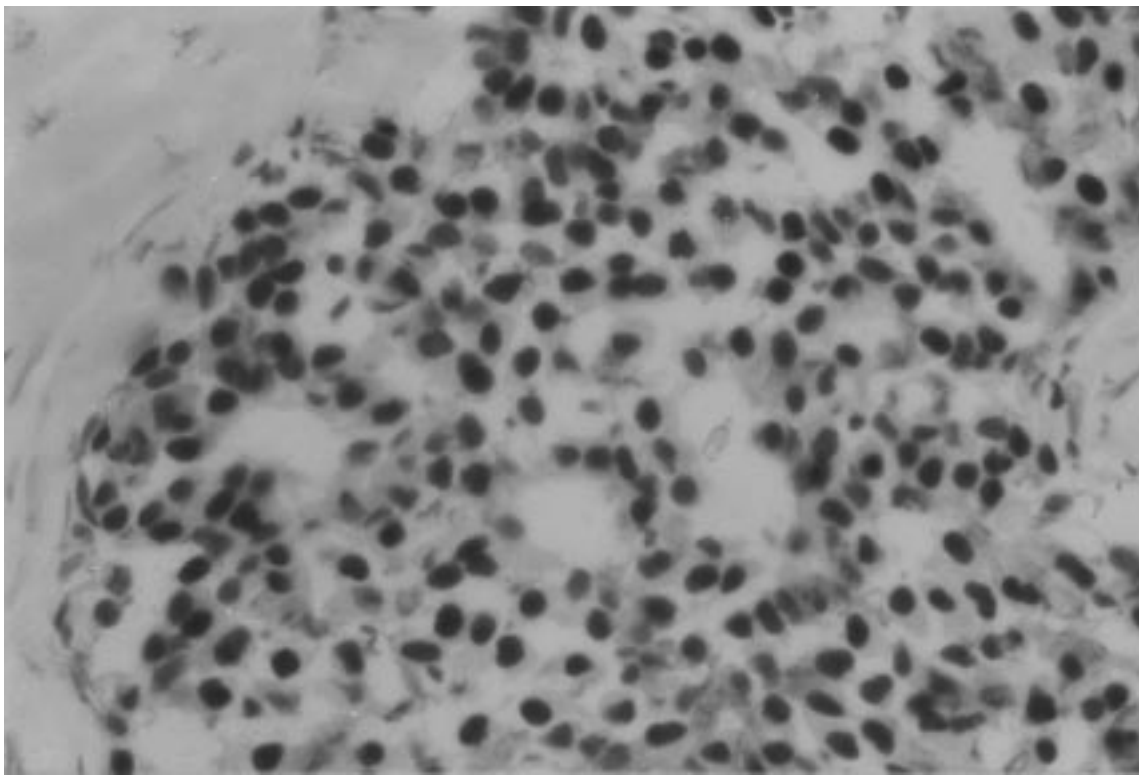
TABLE II
SPEARMAN'S RANK ORDER CORRELATION COEFFICIENT: COMPARISON OF STAINING INTENSITY
CLASS PROPORTIONS FOR ALL IMAGES (** = SIGNIFICANCE BETTER THAN 5% LEVEL)

	negative	weak	moderate	strong	very strong
Expert 1 – Expert 2	0.65*	0.32	0.71*	0.92*	0.76*
BASS – Expert 1	0.58*	0.51*	0.53*	0.83*	0.78*
BASS – Expert 2	0.56*	0.38*	0.81*	0.82*	0.86*

measurements [27], [14]. However, manual assessment of immunolabeled biopsy slides, performed routinely in a majority of pathology laboratories, has been shown to carry diagnostic, prognostic, and therapeutic importance. Nevertheless, Jagoe *et al.* [7] claim that the consensus view of several experts may be the only guide to establishing improved accuracy and reproducibility. In this context a computer-aided system may be viewed as an additional independent expert that can be

used to enhance accuracy. A second run validation experiment showed in a separate study that BASS identified objects the experts missed during the first assessment, leading to an increase in PPV by 12% [28].

In this study BASS' detection system was compared to the detection performance of two human experts. In addition, to analyze the joint performance of detection and classification modules in BASS, the nuclei classification results were cor-



(a)

0 % of nuclei, score 0, are negative (very light gray, original image: blue), score 0:	$0 \cdot 0 = 0$
20 % of nuclei, score 1, are weakly stained (light gray, original image: blue/ brown), score 1:	$1 \cdot 1 = 1$
60 % of nuclei, score 3, are moderately stained (medium gray, original image: light brown), score 2:	$3 \cdot 2 = 6$
20 % of nuclei, score 1, are strongly stained (dark gray, original image: dark brown), score 3:	$1 \cdot 3 = 3$
0 % of nuclei, score 0, are very strongly stained (very dark gray, original image: dark brown), score 4:	$0 \cdot 4 = 0$
Total Score:	10
Diagnostic index:	3+

(b)

Fig. 8. (a) Light micrograph showing immunohistochemical staining of breast cancer nuclei for estrogen receptors (localized gray color; original image: brown color). This case was assigned the diagnostic index of 3+ based on Table IV. (b) The compilation of the diagnostic index, 3+. (Magnification $\times 500$).

related with the experts' nuclei classification results, while the experts' and BASS' diagnostic indices were compared to the routinely derived diagnostic indices. It was shown that BASS has a higher sensitivity to detect nuclei than the experts. Compared to the individual experts, BASS' positive predictive value was low, mainly due to the consistently higher number of detected nuclei by BASS. However, when the detection results from the two experts were merged, BASS' positive predictive value increased to a similar level as that of the experts, which supports the potential of the BASS system to offer increased sensitivity. When comparing BASS' grading and classification performance it was shown that BASS performed best for biopsy slides with a routine diagnostic index of 1+ and 4+, whereas both experts overscored or underscored particularly 1+ and 3+ cases.

Current limitations of the BASS system apply mainly to 1) User interaction: BASS is designed to take advantage of

expert guidance at any desired level of detail regarding both detection and classification of nuclei. In particular, specific subregions of interest may be analyzed separately. 2) Further system validation: Unbiased system validation was performed in this study on a small biopsy database of slides in the sense that BASS was tested without user interaction. However, it is necessary to compare BASS with experts as well as with other commercial systems using a larger biopsy database. Moreover, BASS' assessment results should be correlated with other empirical data, such as survival data, to establish BASS' predictor ability in a clinical environment so that its findings can be compared to other reported methods.

Commercial systems offer a solution to computer-aided biopsy assessment which relies primarily on the global discrimination regarding the field of view between specifically stained nuclear tissue and the background as well as between positively stained (brown) and negatively stained (blue) nu-

TABLE III
CONFUSION MATRICES FOR DIAGNOSTIC INDICES (D.I.) OF 28
BREAST CANCER BIOPSY IMAGES: (a) ROUTINE DIAGNOSTIC
INDEX VERSUS BASS, (b) ROUTINE DIAGNOSTIC INDEX VS. EXPERT
1, AND (c) ROUTINE DIAGNOSTIC INDEX VERSUS EXPERT 2

BASS	Routine Diagnostic Index						
	D. I.	0	1+	2+	3+	4+	Total
	0	-	-	-	-	-	0.0
	1+	10.7	7.1	-	3.6	-	21.4
	2+	3.6	-	10.7	3.6	-	17.9
	3+	-	3.6	14.3	7.1	-	25.0
	4+	-	3.6	-	17.9	14.3	35.7
	Total	14.3	14.3	25.0	32.1	14.3	100

(a)

Expert 1	Routine Diagnostic Index						
	D. I.	0	1+	2+	3+	4+	Total
	0	-	3.6	-	-	-	3.6
	1+	10.7	-	-	-	-	10.7
	2+	3.6	3.6	7.1	3.6	-	17.9
	3+	-	3.6	17.9	3.6	-	25.0
	4+	-	3.6	-	25.0	14.3	42.9
	Total	14.3	14.3	25.0	32.1	14.3	100

(b)

Expert 2	Routine Diagnostic Index						
	D. I.	0	1+	2+	3+	4+	Total
	0	-	3.6	-	-	-	3.6
	1+	14.3	-	-	-	-	14.3
	2+	-	3.6	10.7	-	-	14.3
	3+	-	3.6	3.6	10.7	3.6	21.4
	4+	-	3.6	10.7	21.4	10.7	46.4
	Total	14.3	14.3	25.0	32.1	14.3	100

(c)

clear tissue. Measurements of percent of stained surface area, based on binary masks for nuclear area and positive nuclear area, are the result of global thresholding techniques. One of the advantages of BASS is that it attempts to function as a tool using the same principles as those applied by individual experts. No attempts were made at changing major working principles compared to manual assessment. In particular, BASS detects, counts, and classifies individual nuclei according to the manual semi-quantitative grading scheme. The system is efficient to operate, performing the analysis of one image on average in less than one minute (200-MHz Intel Pentium PC, 32-Mbyte RAM), and can accumulate large samples. Moreover, it assesses the image based on localized operators which allow adaptation not only to local image statistics, but may also give a human expert the opportunity to guide the detection process at the desired level of detail in the context of selecting specific subregions of images for analysis.

The reliability and correctness of assessment results is particularly important in borderline cases where a difference of only one point in the diagnostic index of a biopsy may imply a difference of up to 25% in the expected rate that individual patients may respond to hormonal treatment. Such

cases present the oncologist with difficulties in trying to balance endocrine therapy with adjuvant chemotherapy, or radiotherapy, in an effort to prolong the patient's survival but also minimize the side effects due to overtreatment. In this respect data from BASS may provide a more accurate and efficient means of selecting optimal treatment tailored to individual patients.

There is at present a major effort to standardize immunocytochemical data. However, despite the urgency and need for quantification, there exists no gold standard for immunocytochemically stained biopsy slides, mainly because of a lack of coordination between manufacturers of staining kits, medical institutions, and research laboratories [14]. Therefore, all experiments have to be based on mutual comparisons of two analysis results at a time or be correlated with empirical data stemming from complementary data sources, such as biochemical analysis, tumor staging, or survival rates. The ready availability of data from computer-aided systems will create new opportunities for formulation of guidelines and standardized protocols which are urgently needed in immunocytochemistry [27].

In the future, the system needs to be further validated using larger biopsy databases. Particular emphasis will be placed on the performance comparison with human experts and other commercial systems. A larger database of BASS analyzed cases will help improve its predictive accuracy as compared to conventional methods that are currently in use. In addition, BASS' performance will be further tested on breast cancer cases that have already been analyzed by using both the diagnostic index and commercial systems to calculate its predictive value and performance clinically. Although the present results are based on a small sample pool, BASS performance has been promising and the nuclei detection scheme presented herein has demonstrated a good potential for further validation in immunocytochemistry.

APPENDIX A

SEMI-QUANTITATIVE DIAGNOSTIC INDEX

Routinely, biopsy slides are manually assessed and classified by a human expert with the help of a light microscope [6], [4]. The assessment is based on the intensity of staining and the percentage of cells stained. These two factors are used to calculate the diagnostic index otherwise known as the H-score [5] as illustrated by Fig. 8. This derivation of the H-score may induce interobserver and intraobserver variation errors [7]. Despite these limitations, studies have shown that the results obtained from manual biopsy assessment schemes are clinically important. However, due to the semi-quantitative nature of the manual assessment, there is a need to improve the accuracy, even with scoring schemes that apply five classes for classifying the results.

APPENDIX B

RELATING RECEPTIVE FIELD PARAMETERS TO NUCLEAR SIZE AND INTENSITY

A desired property of a nuclei detection system is a linear dependence of detection on object size, with detection ideally

TABLE IV
COMPUTATION OF MANUAL SEMI-QUANTITATIVE IMMUNOCYTOCHEMICAL DIAGNOSTIC INDEX [4] (SEE EXAMPLE IN FIG. 8)

% of Cells Positive	Score	Staining Intensity	Score	Total Score	Diagnostic Index
0	0	Negative	0	0	0
0 – 25 %	1	Weak	1	1 – 4	1+
26 – 50 %	2	Moderate	2	5 – 8	2+
51 – 75 %	3	Strong	3	9 – 12	3+
≥ 76 %	4	Very Strong	4	≥ 13	4+

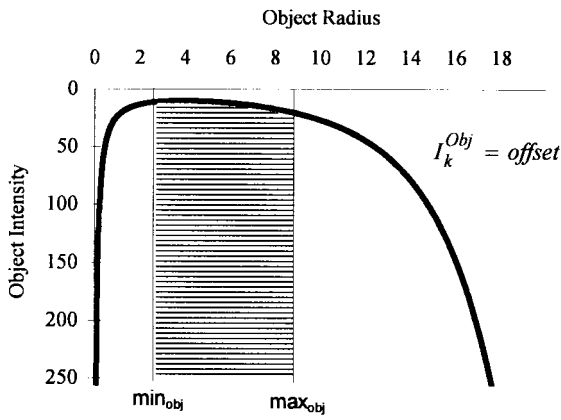


Fig. 9. Receptive field response (B.1) as a function of object size assuming an average object intensity equal to the squashing function with offset = 127.5 and scale = 255. The receptive field parameters e_1 , e_2 , and B were set to 2.5, 7.5, and 3, respectively.

not depending on object intensity. These constraints cannot be optimized for all object sizes simultaneously when receptive fields are used as described. However, parameters can be determined such that the receptive fields have an almost linear response over a desired size range. To select appropriate parameters for a desired range of object sizes, the response of the receptive field in terms of average object intensity can be related to object size (B.1) by modeling nuclei as circular objects with constant intensity. This assumption is reasonable, since the receptive field filter is circularly symmetric. If the convolution integral of the receptive field function from (1) and the object model is evaluated at the origin, the object radius and average object intensity at iteration k can be related to the receptive field parameters and the object intensity at iteration $k+1$ as described by the following equation:

$$I_{k+1}^{Obj}(R^{Obj}) = 4\pi B \left\{ \alpha \rho_1^2 \sqrt{\pi} \cdot \operatorname{erf}\left(\frac{R^{Obj}}{\sqrt{2}\rho_1}\right) - J \rho_2^2 \sqrt{\pi} \cdot \operatorname{erf}\left(\frac{R^{Obj}}{\sqrt{2}\rho_2}\right) \right\} \cdot I_k^{Obj} \quad (\text{B.1})$$

where I_{k+1}^{Obj} depicts the average intensity of the object at iteration k , the rest of the parameters are the same as in (1),

and depicts the well-known error function [26]:

$$\operatorname{erf}(R) = \frac{2}{\sqrt{\pi}} \int_0^R \exp(-u^2) du. \quad (\text{B.2})$$

Fig. 9 shows an example of the dependency of receptive field response on object size for $I_k^{Obj} = \text{offset}$. The response is approximately linear for midrange radii (\min_{obj} to \max_{obj}), while the detection of very small or very large objects depends nonlinearly on size and intensity. Objects, for which the pair (R^{Obj}, I_k^{Obj}) is located below the curve, would only be detected if offset is chosen as the threshold.

ACKNOWLEDGMENT

The authors thank the Pancyprian Association of Cancer Patients and Friends (PASYKAF) for their support and would like to express their gratitude to the reviewers for constructive comments which helped them improve the quality of the paper.

REFERENCES

- [1] F. Schnorrenberg, C. S. Pattichis, K. Kyriacou, M. Vassiliou, and C. N. Schizas, "Computer-aided classification of breast cancer nuclei," *Technol. Health Care*, vol. 4, no. 2, pp. 147–161, 1996.
- [2] L. A. Sternberger, *Immunohistochemistry*. New York: Wiley, 1979.
- [3] L. D. True, "Quantitative immunohistochemistry: A new tool for surgical pathology?," *Am. J. Clin. Pathol.*, vol. 90, no. 3, pp. 324–325, 1988.
- [4] S. Störkel, T. Reichert, K. A. Reiffen, and W. Wagner, "EGFR and PCNA expression in oral squamous cell carcinomas: A valuable tool in estimating the patients prognosis," *Eur. J. Cancer*, vol. 29B, pp. 273–277, 1993.
- [5] K. S. McCarty, Jr., L. S. Miller, E. B. Cox, J. Konrath, and K. S. McCarty, Sr., "Estrogen receptor analysis. Correlation of biochemical and immunohistochemical methods using monoclonal antireceptor antibodies," *Arch. Pathol. Lab. Med.*, vol. 109, pp. 716–721, 1985.
- [6] F. T. Bosman, A. F. P. M. de Goeij, and M. Rousch, "Quality control in immunocytochemistry: Experiences with the oestrogen receptor assay," *J. Clin. Pathol.*, vol. 45, pp. 120–124, 1992.
- [7] R. Jagoe, J. H. Steele, V. Vucicevic, N. Alexander, S. van Noorden, R. Wooton, and J. M. Polak, "Observer variation in quantification of immunocytochemistry by image analysis," *Histochem. J.*, vol. 23, pp. 541–547, 1991.
- [8] Cell Analysis Systems Inc., *Cell analysis systems: Quantitative estrogen progesterone users manual*, Application Version 2.0, Catalog Number 201325-00, Apr. 1, USA, 1990.
- [9] Alcatel TITN Answare, *IMMUNO 4.00: User's guide*, 1st ed., Grenoble, France, Oct. 1993.
- [10] C. Charpin, P. M. Martin, B. DeVictor, M. N. Lavaut, M. C. Habib, L. Andrac, and M. Toga, "Multiparametric study (SAMBA 200) of estrogen receptor immunocytochemical assay in 400 human breast carcinomas:

Analysis of estrogen receptor distribution heterogeneity in tissues and correlations with dextran coated charcoal assays and morphological data," *Cancer Res.*, vol. 48, pp. 1578-1586, 1988.

- [11] G. Brugal, "Color processing in automated image analysis for cytology," *Quantitative Image Analysis in Cancer Cytology and Histology*, J. Y. Mary and J. P. Rigaut, Eds. Amsterdam, The Netherlands: Elsevier, 1985, pp. 19-33.
- [12] S. Bacus and J. L. Flowers, "The evaluation of estrogen receptor in primary breast carcinoma by computer-assisted image analysis," *Am. J. Clin. Pathol.*, vol. 90, pp. 233-239, 1988.
- [13] A. E. Dawson, R. E. Austin, Jr., and D. S. Weinberg, "Nuclear grading of breast carcinoma by image analysis," *Am. J. Clin. Pathol.*, vol. 95 (suppl. 1), pp. S29-S37, 1991.
- [14] D. S. Weinberg, "Quantitative immunocytochemistry in pathology," *Image Analysis: A Primer for Pathologists*, A. M. Marchevsky and P. H. Bartels, Eds. New York: Raven, 1994, pp. 235-260.
- [15] D. H. Hubel and T. N. Wiesel, "Receptive fields, binocular interaction and functional architecture in the cat's visual cortex," *J. Physiol., Lond.*, vol. 160, pp. 106-154, 1962.
- [16] D. H. Hubel, *Eye, Brain, and Vision*. New York: W. H. Freeman, 1988.
- [17] R. W. Rodieck and J. Stone, "Quantitative analysis of cat retinal ganglion cells," *J. Neurophysiol.*, vol. 28, pp. 833-849, 1965.
- [18] D. Marr and E. Hildreth, "Theory of edge detection," *Proc. R. Soc. Lond. B*, vol. 207, pp. 187-217, 1980.
- [19] J. J. Koenderink, "The structure of images," *Biol. Cybern.*, vol. 50, pp. 363-370, 1984.
- [20] A. K. Jain, *Fundamentals of Digital Image Processing*. Englewood Cliffs, New Jersey: Prentice-Hall, 1989.
- [21] J. D. Foley, A. van Dam, S. K. Feiner, and J. F. Hughes, *Computer Graphics: Principles and Practice*, 2nd ed. Reading, MA: Addison-Wesley, 1990.
- [22] D. Travis, *Effective Color Displays: Theory and Practice*. New York: Academic, 1991.
- [23] S. Chen, C. F. N. Cowan, and P. M. Grant, "Orthogonal least squares learning algorithm for radial basis function networks," *IEEE Trans. Neural Networks*, vol. 2, no. 2, pp. 302-309, 1991.
- [24] MathWorks Inc., *Neural Network Toolbox User's Guide*, Version 1.0, Jan., 1994.
- [25] F. Schnorrenberg, "Comparison of manual and computer-aided breast cancer biopsy grading," in *Proc. IEEE EMBS '96, 18th Annu. Int. Conf.*, Amsterdam, The Netherlands, 1996, paper no. 556.
- [26] W. H. Press, B. P. Flattery, S. A. Teukovsky, and W. T. Vetterling, *Numerical Recipes in C*. Cambridge, U.K.: Cambridge Univ. Press, 1988.
- [27] C. R. Taylor, "An exaltation of experts: Concerted efforts in the standardization of immunohistochemistry," *Appl. Immunohistochem.*, vol. 1, pp. 232-243, 1993.
- [28] F. Schnorrenberg, N. Tsapatsoulis, C. S. Pattichis, C. N. Schizas, S. Kollias, M. Vassiliou, A. Adamou, and K. Kyriacou, "A modular neural network system for the analysis of nuclei in histopathological sections," Tech. Rep. TR-97-2, Dept. Comput. Sci., University Cyprus, Jan. 1997. (Also submitted to *IEEE Engineering in Medicine and Biology Magazine*.)



Frank Schnorrenberg (S'93) received the M.Sc. degree in computer science from Texas A&M University, College Station, TX, in 1992. He is currently pursuing the Ph.D. degree in computer science.

From 1988 to 1990, he worked for the German National Research Center for Information Technology (GMD), St. Augustin, Germany, as a Research Student in the area of non-monotonic logics and truth maintenance systems. From 1991 to 1992, he was a Research Assistant and Research Associate in the Petroleum Engineering Department, Texas

A&M University, working on the detection of fractures in sonic borehole image data utilizing neural network technology. In 1993, he joined the Department of Computer Science, University of Cyprus, as a Research Associate working in the area of medical image analysis and neural networks. His research interests include computationally intelligent systems, medical image analysis, health telematics, and diagnostic and prognostic systems.

Mr. Schnorrenberg was the recipient of a Fulbright scholarship during his stay at Texas A&M University from 1990 to 1992.



Constantinos S. Pattichis (S'84-M'88) was born in Nicosia, Cyprus, on June 30, 1959. He received the B.Sc. degree in electrical engineering from the University of New Brunswick, Fredericton, N.B., Canada, in 1983, the M.Sc. degree in biomedical engineering from the University of Texas at Austin in 1984, the M.Sc. degree in neurophysiology from the University of Newcastle upon Tyne, U.K., in 1988, and the Ph.D. degree in electronic engineering from the University of London, U.K., in 1992.

From 1985 to 1992 he was working with the Cyprus Institute of Neurology and Genetics, where he is now a Visiting Senior Scientist. He is also currently an Assistant Professor with the Department of Computer Science at the University of Cyprus, Nicosia, and is actively participating in a number of European projects related to health telematics. His current research interests include medical imaging, biosignal analysis, artificial neural networks, and genetic algorithms. He has published over 40 refereed journal and conference papers in these areas.

Dr. Pattichis has been involved in numerous professional society activities, including President of the Cyprus Association of Medical Physics and Biomedical Engineering, 1996-1998, Vice-president of the IEEE Cyprus Section, 1996-1998; and General Co-Chairman, Medical and Biological Engineering and Computing Conference 98 (Medicon'98). He was the recipient of the 1994 European Community "Marie-Curie" fellowship.



Kyriacos C. Kyriacou was born in Nicosia, Cyprus, in 1954. He received the B.Sc. degree in biochemistry from the University of London, U.K., in 1977 and the Ph.D. degree from King's College Medical School, London, in 1982. During his Ph.D. research he specialized in the use of histopathological techniques, including electron microscopy, for diagnostic as well as for research applications.

In 1982, he was appointed lecturer at King's College Hospital Medical School. Since 1991, he has been working at the Cyprus Institute of Neurology and Genetics as a Senior Scientist. He established the first Electron Microscope Department in Cyprus, which offers a centralized diagnostic service for the whole island. His research interests include quantitative imaging of histopathological features as well as cancer genetics.



Christos N. Schizas (M'83-SM'91) received the B.Sc. degree in electronic engineering from the University of London, U.K., in 1978, the M.B.A. degree from Indiana University, Bloomington, in 1988, and the Ph.D. degree in systems theory from the University of London, U.K., in 1981.

He was a Postdoctoral Fellow at the University of London from 1981 to 1983, taught as Lecturer of Computer Science at the Higher Technical Institute of Cyprus from 1985 to 1990, and was Professor of Computer Information Systems at Indiana University from 1990 to 1992. Since 1992, he has been with the Department of Computer Science, University of Cyprus, Nicosia, as Associate Professor, where he served as Interim Chair of the department until 1994. He is also the Director of Computational Intelligence Research at the Cyprus Institute of Neurology and Genetics. His research interests include computational intelligence, decision support systems, medical applications, and diagnostic systems. He has published over 70 refereed journal and conference papers in these areas.

Dr. Schizas is a Fellow of the IEE and BCS, and since 1992 has been a Member of the International Committee of the IEEE-EMBS annual conference. He is a member of the ministerial committee for establishing the Information Society in Cyprus, and partner in various European Union-funded projects. He received the 1979 William Lincoln Shelley award from the University of London for excellence in research, and a Fulbright fellowship for collaborative research in the United States in 1993.